Design of the tip state estimator for hybrid-structured flexible manipulator based on SDFT and FLAKF

Teng Long
The State Key Laboratory of Management and Control for Complex Systems, Institute of Automation, Chinese Academy of Sciences, Beijing, China and University of the Chinese Academy of Sciences, Beijing, China, and
En Li, Junfeng Fan, Lei Yang and Zize Liang
Institute of Automation Chinese Academy of Sciences, Beijing, China and University of the Chinese Academy of Sciences, Beijing, China

Abstract

Purpose – This paper aims to design a tip state estimation method for a hybrid-structured flexible manipulator (HSFM) with one rotating joint and one telescopic joint in the vertical plane.

Design/methodology/approach – The HSFM model is decomposed into a static deflection model and a vibration model. The sliding discrete Fourier transform (SDFT) is used to filter the high frequency noise and obtain main vibration components to represent the vibration model. Then, a novel fuzzy logic adaptive Kalman filter (FLAKF) is designed to estimate the state of a vibrational equilibrium position. The complete tip state of the HSFM is obtained by superimposing the FLAKF filter results with the SDFT vibration analysis results.

Findings – Both the simulation results and physical experimental results verify the effectiveness of the proposed tip state estimation method. The vibration analysis based on SDFT is used to represent the vibration model and reduce the computational complexity in the process of solving differential equation. The proposed FLAKF can effectively increase the stability and robustness of the estimator.

Originality/value – In this paper, the tip state estimation problem of the HSFM in vertical plane is first proposed. The effect of gravity on the HSFM is considered by the static deflection model. A precise tip state estimator is designed by a closed loop SDFT and a novel FLAKF, which can provide an accurate feedback for the vibration control controller and make an accurate evaluation of the control effect.

Keywords Fuzzy logic adaptive Kalman filter (FLAKF), Hybrid-structured flexible manipulator (HSFM), Sliding discrete Fourier transform (SDFT), Tip state estimator

Paper type Research paper

1. Introduction

The flexible manipulator has many advantages, such as large load and mass ratio, large working space, fast moving speed, small actuators, low energy consumption and good operability. It has a wide application prospects in fields of space exploration, architecture and nuclear industry. But the flexible manipulator has the structural characteristics, such as low stiffness, large deflection, nonlinearity, low damping and low natural frequency. Therefore, it is easy to cause low frequency and large vibration during the motion process. These problems will affect the positional accuracy and track tracking accuracy of the flexible manipulator. In the case of large amplitude, it may cause a safety accident. Therefore, the research on the control of the vibration suppression of the flexible manipulator is the key to improve its performance. In recent years, many researchers have done a lot of work on modeling, control and trajectory planning of flexible manipulator, which were introduced and summarized in the review papers of Benosman and Le Vey (2004), Dwivedy and Eberhard (2006), Kiang *et al.* (2015) and Sayahkarajy *et al.* (2016).

But in the research of flexible manipulator, most of research objects are single link or multi-link flexible manipulator (Zhu *et al.*, 1999; Benosman *et al.*, 2003; Malgaca *et al.*, 2016; Chen *et al.*, 2017; Yang and Tan, 2018). These structures are relatively simple, and they cannot accurately reflect the characteristics of the flexible manipulator in the practical application. In addition, most of the researches of flexible manipulator only consider the rotation motion in the horizontal plane, such as researches of Yang and Tan (2018), Abe (2010), Mirzaee *et al.* (2010), Feliu *et al.* (2012) and Yavuz *et al.* (2016). To simplify the analysis process, the influence of gravity is ignored in most researches (Abe, 2010; Mirzaee *et al.*, 2010; Sooraksa and Chen, 1998; Lou *et al.*, 2015). This kind of flexible manipulator without considering the influence of gravity has great research

The current issue and full text archive of this journal is available on Emerald Insight at: **www.emeraldinsight.com/0144-5154.htm**

Assembly Automation
38/5 (2018) 576–586

[DOI 10.1108/AA-12-2017-192]

This project was supported by the National Natural Science Foundation of China (Grant No. U1713224).

Received 28 December 2017
Revised 31 March 2018
13 April 2018
Accepted 11 May 2018

significance in the field of space exploration, but the flexible manipulator applied in the field of architecture and nuclear industry cannot ignore the influence of gravity (Carlos and Feliu, 2017). In this paper, a hybrid-structured flexible manipulator (HSFM) with a telescopic joint and a rotating joint in the vertical plane is first considered as the research object. The advantages of the hybrid structure are larger workspace and lower system energy consumption. The influence of gravity must be considered in the flexible manipulator moving in a vertical plane, which is a big attempt in this field.

In the closed loop control system of the HSFM, the tip state needs to be fed back in real time and the precise tip state is the basis of precise control. There are strong coupling relations between the two joints of HSFM, and inertia, friction, joint clearance and input and output saturation cannot be accurately obtained. Therefore, the dynamics model established by theoretical method cannot get the tip state of HSFM accurately. When the rotation angular position is different, the tip deflection of the HSFM will be different because of the influence of gravity. In addition, the vibration of HSFM is usually mixed with multiple frequencies during the motion process. If the amplitude and frequency of the main vibration cannot be obtained, it is difficult to get the precise tip state. The location of the sensor and the noise of the measured signal will also cause the deviation between the measured value and the actual value.

At present, researchers have done much work on the analysis method for pure vibration signal (Yang *et al.*, 2017; Trapero *et al.*, 2007; Ziarani and Konrad, 2004; Hou, 2005; Hsu *et al.*, 1999; Sumathi and Janakiraman, 2008; Shitole and Sumathi, 2015). Trapero accurately estimated the vibration frequency by using algebraic identification. The algebraic identification has fast convergence speed, but it cannot get the amplitude of the vibration signal (Trapero *et al.*, 2007). Ziarani adopted the adaptive nonlinear estimator to accurately analyze the vibration frequency (Ziarani and Konrad, 2004). Hou and Hsu used the global convergence identification method to deal with the noise and phase bias of the signal, but the response speed was slow (Hou, 2005; Hsu *et al.*, 1999). Sumathi used the sliding Fourier transform to estimate the amplitude and frequency accurately, and this method can deal well with the noise (Sumathi and Janakiraman, 2008; Shitole and Sumathi, 2015).

In the research of filtering algorithms, Kalman filter was widely used, and a number of Kalman filtering algorithms which are more robust to nonlinear systems have been derived, such as extended Kalman filter (EKF), Sage-Husa adaptive Kalman filter, unscented Kalman filter, central difference Kalman filter and so on. All kinds of the improved Kalman filtering algorithms can improve the accuracy and the stability of filtering, but they also have some limitations. The EKF requires that the state equation must be continuously differentiable, and the estimation precision is reduced when the system has strong nonlinearity. Sage-Husa adaptive Kalman filter also exists some defects, such as high computational complexity, easy divergence of state estimation and poor robustness (Bian *et al.*, 2006). When the nonlinearity is strong, the noise covariance matrix is easily changed into a negative definite matrix, which makes the filter unstable. The center difference Kalman filter is not suitable for the situation where the precision of the estimation is very high.

In this paper, a tip state estimation method of the HSFM based on fuzzy logic adaptive Kalman filter (FLAKF) and sliding discrete Fourier transform (SDFT) is designed. The static deflection model of the HSFM is established, and the main vibration components of the tip are separated by SDFT, which are used to replace the vibration model of the system. After filtering the original signal in frequency domain, the proposed FLAKF is used to estimate the data after filtering in frequency domain, and the state of a vibrational equilibrium position is obtained. Finally, the vibration signal and the equilibrium position of the vibration are superimposed to get the complete tip state.

The rest of the paper is organized as follows: In Section 2, the static deflection model of the HSFM and the state equation are introduced. In Section 3, the overall structure of the estimator is introduced, and the vibration analysis based on SDFT and the FLAKF algorithm are described. In Section 4, the simulation experiments are designed, the experimental device is introduced and the experimental results are analyzed to verify the effectiveness of the proposed method. Finally, the conclusions are drawn in Section 5.

2. System model

In general, to estimate the tip state of HSFM accurately, it is necessary to establish the kinematics and dynamics model of HSFM. But for an elastic system with complex structures, the dynamics model is highly nonlinear and strongly coupled, and the accurate system model is difficult to be obtained according to the existing researches (Chen, 2001; Vartanov *et al.*, 2017). Therefore, a complete dynamics model of HSFM is not applicable in the state estimation process. In this paper, the HSFM model is decomposed into a rigid system model and an elastic vibration model to estimate the tip state. The tip deflection of the HSFM increases with the extension of the telescopic joint and the load weight, and it also varies with the angle of rotation. Therefore, the static deflection model should be considered. In addition, to reduce the computational complexity, the vibration signals are analyzed, and the vibration model is replaced by the vibration analysis results. The tip state estimate model of the HSFM is shown as Figure 1.

2.1 Static deflection model

The telescopic joint of HSFM is divided into three segments, which are the foundation segment, the overlap segment and the

Figure 1 The HSFM tip state estimate model

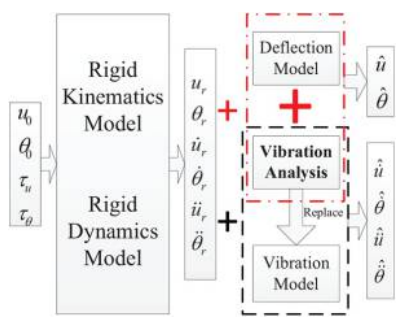

extension segment, shown in Figure 2. The deflection is calculated for each segment by the theory of cantilever beam (Long *et al.*, 2016). When the deflection of the foundation segment is calculated, the overlap and extension segments are considered as the load. In the same way, when the deflection of the overlap segment is calculated, the extension segment is considered as the load.

According to the modeling method in the researches of Liu *et al.* (2011), Makarov *et al.* (2012) and Bosman *et al.* (2015), the coordinate system is set up on the model of HSFM. w_1, w_2 and w_3 represent the maximum elastic deviation of each segment, l_1, l_2 and l_3, respectively, represent the length of each segment. Because the vibration is mainly caused by the rotation motion, we assume that the elastic vibration occurs only in the direction of rotation. θ_1 represents the rotation angle of the rotating joint, u represents the extension length of the second flexible link, τ represents the input torque of the rotating joint and the F represents the driving force of the telescopic joint. θ_2 and θ_3 represent the joint angle of overlap and extension segments, and θ represents the tip joint angle of the HSFM.

For a stationary state cantilever beam with uniform mass distribution and load, the tip deflection can be expressed by equation (1):

$$W_{\max} = \frac{ql^4}{8EI} + \frac{Fb^2}{6EI}(3l - b). \tag{1}$$

where q is the gravity of the link of unit length, l is the length of the flexible link, E is the elastic modulus, I is the cross-section inertia moment, F is the tip external force and b is the force arm acting on F.

According to equation (1), the deflection of the foundation segment, the overlap segment and the extension segment can be expressed as:

$$W_1 = \cos\theta_1\left[\frac{\rho_1 g(l_1+u)^4}{8EI_1} + \frac{(\rho_1+\rho_2)(l_2-u)g(2l_1+l_2+u)^2(4l_1-l_2+5u)}{48EI_1}\right] + \cos\theta_1\frac{\rho_3(l_3+u)g(2l_1+2l_2+l_3+u)^2(4l_1-2l_2-l_3+5u)}{48EI_1}, \tag{2}$$

$$W_2 = \cos\theta_1\left[\frac{(\rho_1+\rho_2)g(l_2-u)^4}{8EI_2} + \frac{\rho_3(l_3+u)g(2l_2+l_3-u)^2(4l_2-l_3-5u)}{48EI_2}\right], \tag{3}$$

$$W_3 = \cos\theta_1\frac{\rho_2 g(l_3+u)^4}{8EI_3}. \tag{4}$$

So the static deflection at the tip of the HSFM can be expressed as:

$$W = W_1 + W_2 + W_3. \tag{5}$$

2.2 System state equation

According to the rigid model and the static deflection model of the system, we know that the tip state of the HSFM is a nonlinear function. Considering the system noise, the state equation of the system can be expressed as follows:

$$\mathbf{x}(t_{k+1}) = f[\mathbf{x}(t_k), \mathbf{u}(t_k)] + \mathbf{q}(t_k). \tag{6}$$

where t_k represents an arbitrary discrete moment, and $\mathbf{x}(t_k)$ represents the tip state vector at the t_k moment, including the position, speed and acceleration in the direction of rotation and telescopic. $\mathbf{u}(t_k)$ represents the output torque of the rotating joint and the telescopic joint at the t_k moment, and $\mathbf{q}(t_k)$ represents the

Figure 2 Schematic diagram of hybrid structure flexible manipulator

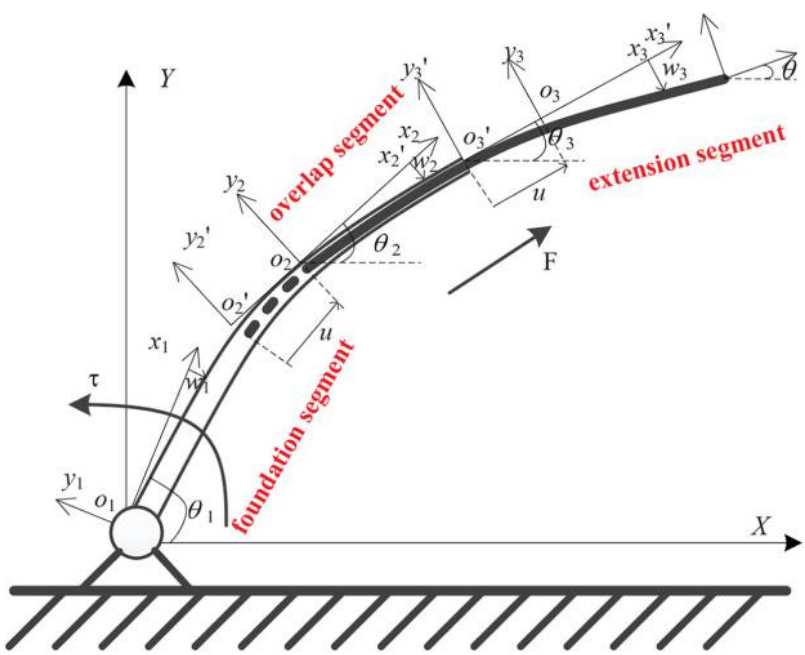

system error vector at the t_k moment. Equation (6) is expanded by the Taylor formula, and the first-order linear expression is taken into account, and the HSFM linear state equation is obtained:

$$\mathrm{x}(t_{k+1}) \approx \hat{\Phi}(t_k)\mathrm{x}(t_k) + \left[f(\hat{\mathrm{x}}(t_k), \mathrm{u}(t_k)) - \hat{\Phi}(t_k)\hat{\mathrm{x}}(t_k)\right] + \mathrm{q}(t_k), k = 0, 1, 2 \ldots \tag{7}$$

In equation (7):

$$\hat{\Phi}(t_k) = \frac{\partial f[\mathrm{x}(t_k), \mathrm{u}(t_k)]}{\partial \mathrm{x}(t_k)}\Big|_{\mathrm{x}(t_k)=\hat{\mathrm{x}}(t_k)}. \tag{8}$$

The state transition matrix of the system can be represented as equation (8).

According to the characteristics of the attitude sensor, the measurement equation is set up as follows:

$$y(t_k) = \mathrm{H}(t_k)\mathrm{x}(t_k) + \mathrm{r}(t_k). \tag{9}$$

where $\mathrm{y}(t_k)$ represents the measurement vector of attitude sensor at the t_k moment, $\mathbf{H}(t_k)$ represents the measurement coefficient matrix at the t_k moment and $\mathbf{r}$ (t_k) represents the measurement noise vector at the t_k moment.

It is assumed that the expectation and covariance matrix of the system noise and the measured noise are shown as follows:

$$E[\mathrm{q}(t_k)] = \hat{\mathrm{q}}(\mathrm{t}_k), E[\mathrm{r}(\mathrm{t}_k)] = \hat{\mathrm{r}}(\mathrm{t}_k). \tag{10}$$

$$\begin{aligned} Cov\left[\mathrm{q}(t_k), \mathrm{q}(t_j)\right] &= \hat{\mathrm{Q}}(t_k)\delta_{t_k t_j} \\ Cov\left[\mathrm{r}(t_k), \mathrm{r}(t_j)\right] &= \hat{\mathrm{R}}(t_k)\delta_{t_k t_j}. \end{aligned} \tag{11}$$

$$\delta_{t_k t_j} = \begin{cases} 0, & t_k \neq t_j \\ 1, & t_k = t_j. \end{cases} \tag{12}$$

Because the noise of the attitude sensor has a direct relationship with the environment in which it is located, the noise covariance cannot be regarded as a constant. By selecting the appropriate initial value, the convergence speed of the filtering algorithm can be accelerated. Therefore, before the HSFM motion, the sensor data are collected, and the mean and variance of noise are estimated. The estimated results are used as the initial value of the expectation and covariance.

3. State estimator

Due to the inaccuracy of the system model, there is an error between the tip calculation value by the system model and the actual value. In this paper, attitude sensor, accelerometer and encoders are used to measure the state of the system. The attitude sensor is used to measure the angle between the tip of HSFM and the horizontal plane, but there will be a cumulative error. In addition, the tip deflection of HSFM changes with the motion of the telescopic joint and the weight of the tip load, and the accelerometer has baseline drift and measurement noise (Yi *et al.*, 2010; Coelho *et al.*, 2011). So the tip state cannot be accurately measured by these sensors. Moreover, the direct application of Kalman filter algorithm cannot distinguish the vibration and noise. The encoders installed in the rotating joint and the telescopic joint can accurately measure the motion of the joint. This measured value is an important reference for the tip state estimation.

In this paper, the vibration signal is analyzed by SDFT, and the vibration model is replaced by the analysis result. The SDFT is used to separate the main vibration components in the tip state signal and filter the measured data by attitude sensor in the frequency domain. The filtered data are estimated by the FLAKF, which can effectively improve the estimation accuracy.

3.1 Estimator structure

Through the static deflection model, sensor measurement data, SDFT vibration analysis and FLAKF, the final state estimation value can be obtained. The encoder data are used as the reference data of the estimator to avoid large estimated deviation. By combining the rigid model and the static deflection model, the theoretical results of the equilibrium position of the vibration can be obtained efficiently. The separation of vibration signals by SDFT can effectively avoid the problems of high computational complexity and low precision in the process of estimation. Compared with the other adaptive Kalman filtering algorithm, FLAKF can adjust the expectation and covariance of the system noise and measurement noise simultaneously and obtain the HSFM tip state more accurately. The complete estimator structure is expressed in Figure 3.

3.2 Vibration analysis

To meet the requirements of real-time estimation of HSFM, a vibration analysis method based on SDFT is adopted in this paper, which can effectively reduce the computational complexity. The discrete Fourier transform (DFT) can only calculate the entire signal spectrum, while SDFT uses a single frequency unit calculation. Therefore, SDFT can calculate the entire spectrum, or calculate part of the spectrum according to the actual needs, which greatly improves the flexibility of spectral analysis.

To ensure the stability of SDFT, the discount factor r is introduced, and the corresponding differential equation of SDFT is as follows (Sumathi and Janakiraman, 2008; Shitole and Sumathi, 2015):

$$Y_k(n) = \left[Y_k(n-1) + x_a(n) - r^N x_a(n-N)\right] r e^{j2\pi k/N}. \tag{13}$$

According to equation (13), the next time point spectrum can be obtained only by two real number addition and one complex

Figure 3 The complete estimator structure

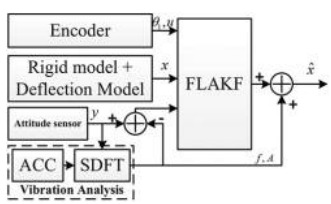

multiplication. k represents time index, $x_a(n-N)$ represents the signal of tip delay, $Y_k(n)$ represents DFT of point n and $Y_k(n-1)$ is the DFT of the previous point.

The structure of SDFT single frequency unit is shown in Figure 4.

As shown in Figure 4, the single frequency unit of SDFT algorithm is composed of a comb filter and a complex resonator. If all N point spectrum components are needed, N complex resonators are required. (Jacobsen and Lyons, 2003; Jacobsen and Lyons, 2004).

The Z transformation is performed in equation (13), the transfer function is obtained as follows:

$$H_k(z) = \frac{(1 - r^N z^{-N})(e^{j2\pi k/N})}{1 - re^{j2\pi k/N} z^{-1}}, 0 < r < 1. \quad (14)$$

In equation (14), the denominator has N zero points with the same spacing in the unit circle of the Z domain, and the molecule has a monopole point $z = e^{j2\pi k/N}$. The discount factor r makes the zero points and poles points within the unit circle to ensure that the output of the SDFT filter is stable. On the premise of the filter stability, the value of r should be as close to 1 as possible to realize error minimization. The real part and the imaginary part of the transfer function $H_k(z)$ can be expressed as:

$$\mathrm{Re}[H_k(z)] = \frac{(1 - r^N z^{-N})\left(r\cos(2\pi k/N) - r^2 z^{-1}\right)}{1 - 2r\cos(2\pi k/N) z^{-1} + r^2 z^{-2}}. \quad (15)$$

$$\mathrm{Im}[H_k(z)] = \frac{(1 - r^N z^{-N})(r\sin(2\pi k/N))}{1 - 2r\cos(2\pi k/N) z^{-1} + r^2 z^{-2}}. \quad (16)$$

The vibration frequency of HSFM is not a constant, and the sampling frequency and the signal frequency must be matched each other to reduce the frequency leakage. The traditional SDFT adopts an open loop analysis method and the problem of frequency drift cannot be solved. In this paper, a closed loop SDFT algorithm is used to adjust the sampling frequency in real time so that the sampling frequency and the signal frequency match each other.

The structure of the closed loop SDFT algorithm is shown in Figure 5.

The closed loop structure includes the phase detector, the moving average filter (MAF), the PI controller and the numerically controlled oscillator (NCO). The phase detector is used to compare the phase difference between the SDFT base frequency signal and the actual input signal. Because the phase difference is proportional to the frequency difference, the relation of the frequency difference e is also obtained (Shitole and Sumathi, 2015). The MAF is used to smooth the frequency difference obtained by the phase detector. The output signal u_o of the PI controller is obtained according to the $\bar{e}$ and the maximum sampling frequency (Turner, 2003).

To obtain multi-order frequency characteristics, multiple resonator units are constructed and the amplitude and frequency of the N point are calculated respectively. According to equation (14), the comb filter is independent of k. To simplify the calculation, all resonators share a comb filter. The structure of the vibration analysis process is shown in Figure 6.

Figure 4 The single frequency unit of SDFT

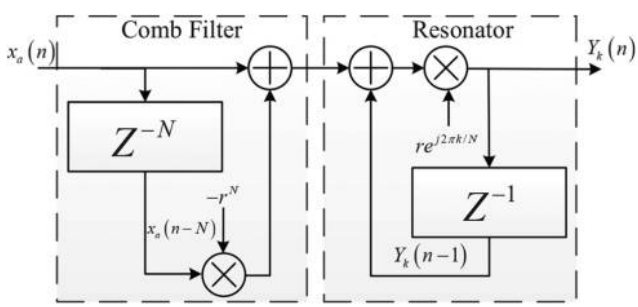

Figure 5 The closed loop SDFT algorithm

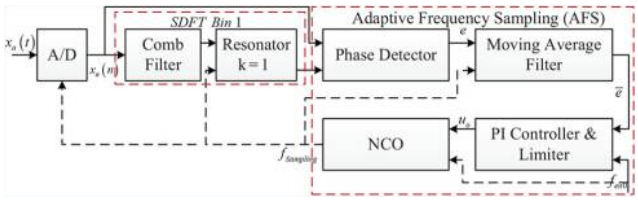

3.3 Fuzzy logic adaptive Kalman filter

In this paper, a new FLAKF is designed based on Sage-Husa adaptive filter (Lu *et al.*, 2007; Yang and Gao, 2006). The adaptive filter can estimate the expectation and covariance matrix of the measured noise and the system noise in real time, and it is more robust.

According to the EKF algorithm and Sage–Husa adaptive filtering algorithm, the whole process of filtering can be divided into time updating process and state updating process:

$$\hat{\mathrm{x}}(t_k|t_{k-1}) = f[\mathrm{x}(t_{k-1}), \mathrm{u}(t_{k-1})] + \hat{\mathrm{q}}(t_k). \quad (17)$$

$$\mathrm{P}(t_k|t_{k-1}) = \hat{\Phi}(t_k|t_{k-1})\mathrm{P}(t_{k-1})\hat{\Phi}(t_k|t_{k-1})^T + \hat{\mathrm{Q}}(t_{k-1}). \quad (18)$$

$$\hat{\mathrm{x}}(t_k) = \hat{\mathrm{x}}(t_k|t_{k-1}) + K(t_k)\tilde{\mathrm{z}}(t_k). \quad (19)$$

$$\tilde{\mathrm{z}}(t_k) = \mathrm{y}(t_k) - \mathrm{H}(t_k)\hat{\mathrm{x}}(t_k|t_{k-1}) - \hat{\mathrm{r}}(t_k). \quad (20)$$

Figure 6 The structure of SDFT

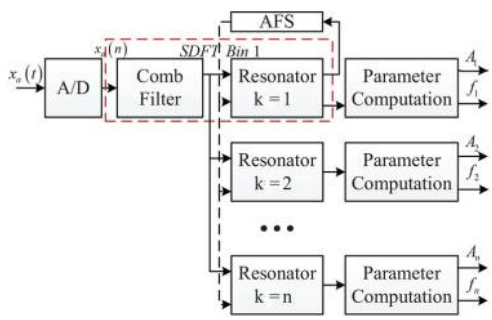

$$K(t_k) = \mathrm{P}(t_k|t_{k-1})\mathrm{H}(t_k)^T\left[\mathrm{H}(t_k)\mathrm{P}(t_k|t_{k-1})\mathrm{H}(t_k)^T + \hat{\mathrm{R}}(t_k)\right]^T. \quad (21)$$

$$\mathrm{P}(t_k) = \left[\mathrm{I} - K(t_k)\mathrm{H}(t_k)\right]\mathrm{P}(t_k|t_{k-1}). \quad (22)$$

The covariance of the innovation in the filtering process is expressed as follows:

$$\mathrm{P}_z(t_k) = \mathrm{H}(t_k)\mathrm{P}(t_k|t_{k-1})\mathrm{H}(t_k)^T + \hat{\mathrm{R}}(t_k). \quad (23)$$

The time updating process can be represented with equations (17) and (18), and the predicted value $\hat{\mathrm{x}}(t_k|t_{k-1})$ of the system state and the predicted value $\mathrm{P}(t_k|t_{k-1})$ of covariance are obtained. The state updating process can be represented with equations (19)-(22), the estimated value $\hat{\mathrm{x}}(t_k)$ of the system state and the estimated value $\mathbf{P}(t_k)$ of covariance are obtained. The $\mathrm{K}(t_k)$ in equation (21) is the Kalman gain at the t_k moment.

The expectation and covariance of system noise and measurement noise $\hat{\mathrm{q}}(t_k)$, $\hat{\mathrm{r}}(t_k)$, $\hat{\mathrm{Q}}(t_k)$ and $\hat{\mathrm{R}}(t_k)$ need to be estimated in real time. According to the traditional Sage–Husa adaptive filtering algorithm, the expectation of system noise and measurement noise are obtained by equations (24) and (25):

$$\hat{\mathrm{q}}(t_k) = \left(1 - d(t_k)\right)\hat{\mathrm{q}}(t_{k-1}) + d(t_k)\left[\hat{\mathrm{x}}(t_k) - \hat{\Phi}(t_k|t_{k-1})\hat{\mathrm{x}}(t_{k-1})\right]. \quad (24)$$

$$\hat{\mathrm{r}}(t_k) = \left(1 - d(t_k)\right)\hat{\mathrm{r}}(t_{k-1}) + \mathrm{d}(t_k)\left[y(t_k) - \mathrm{H}(t_k)\hat{x}(t_k|t_{k-1})\right]. \quad (25)$$

$$\mathrm{d}(t_k) = (1-b)/(1-b^{t_{k+1}}). \quad (26)$$

The $0 < b < 1$ is called a forgetting factor, and the d is gradually reduced and approximated to the $1-b$ when time t_k increases.

In this paper, the fuzzy logic algorithm is used to estimate the covariance $\hat{\mathrm{Q}}(t_k)$ and $\hat{\mathrm{R}}(t_k)$ of the system noise and measurement noise to reduce the computational complexity and improve the robustness of the estimator. The input of the fuzzy logic is the covariance and the expectation of the innovation and the output is the weight α.

It is assumed that the covariance of the system noise and the covariance of the measurement noise are as follows:

$$\hat{\mathrm{Q}}(t_k) = \mathrm{Q}\alpha^{-2(t_k+1)}. \quad (27)$$

$$\hat{\mathrm{R}}(t_k) = \mathrm{R}\alpha^{-2(t_k+1)}. \quad (28)$$

In equations (27) and (28), **Q** and **R** are constant matrices. If α is greater than 1 when time t_k increases, $\hat{Q}(t_k)$ and $\hat{R}(t_k)$ decrease, and the weight of the new measured values increase.

The designed fuzzy rules are as follows:

According to the analysis of the measured data, the expectation and covariance of the innovation are less than 4. Therefore, the expectation and covariance of the innovation are divided into three feature sets {zero, small, large}, and the output weight is divided into four feature sets {zero,small,medium,large}. The subsection functions are used as a membership functions, which are expressed as shown in Figure 7.

In general, the Kalman filter becomes unstable when the covariance of the innovation becomes larger and the expectation gets farther away from the zero. In this case, a larger weight is added to ensure that all the states of the model can be fully stimulated by the system noise, so α should be assigned as a large value. When the covariance and expectation are very large, the measurement data are abnormal, and the filter cannot rely on the measured data, so α should be assigned as a zero value. According to the above analysis, the fuzzy inference rules are designed, and they are shown in Table I.

The centroid method is used to defuzzification for the result of fuzzy inference rules, and the exact output value α is obtained.

3.4 Design of closed loop control system

In view of the fact that the true value of tip state cannot be obtained accurately during motion process, a closed control system is designed to verify effectiveness of the estimator indirectly. The output of the estimator is used as the feedback of the controller, and the tracking performance of the different estimator as feedback is observed under the same control algorithm. The structure of the designed control system is shown in Figure 8.

The PD control algorithm is used as the trajectory tracking control algorithm of the system. The input of the control system is the tip reference trajectory of the HSFM, and the input of the PD controller is the error of the estimator output and the reference trajectory. The joint torque is adjusted by the PD controller to achieve better tracking effect. The EKF estimator and the proposed estimator in this paper are applied to the control system, and the tracking effect of the system is

Figure 7 Fuzzy logic membership function

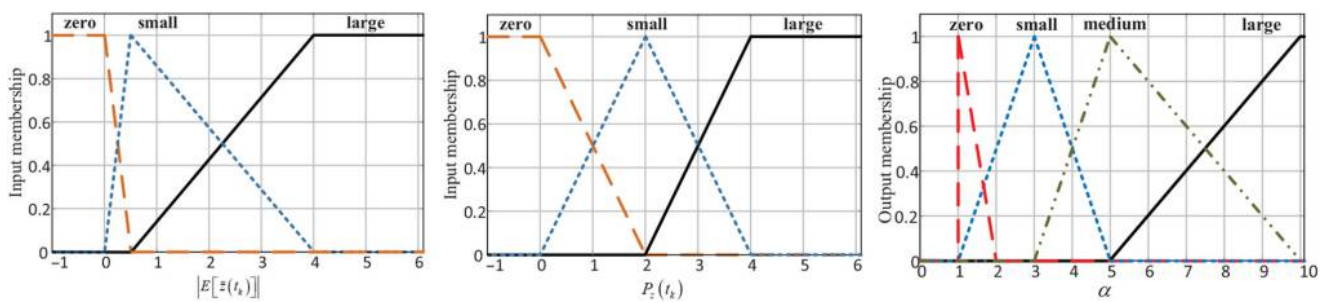

Table I the Fuzzy inference rules

α		zero	$\lvert E[\tilde{z}(t_k)]\rvert$ small	large
$P_z(t_k)$	zero	small	zero	large
	small	zero	large	medium
	large	large	medium	zero

Figure 8 The closed control system of HSFM

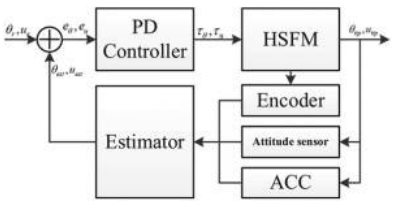

compared in case of the different estimator. If the tracking effect obtained by the proposed estimator is better, the estimator is more accurate.

4. Simulation and experiment

4.1 Simulation result

According to the model of HSFM and the measurement characteristics of the sensor, a signal with Gauss noise and multi-frequency vibration is designed. The original signal s_1, without noise and vibration, is a sinusoidal signal with a frequency of 2Hz and amplitude of 3 cm, and it is shown in equation (29):

$$s_1 = 3\sin(4\pi t). \tag{29}$$

The Gauss noise s_2 obeys $N(\mu, \delta^2)$, the mean μ obeys U (0,0.1) and standard deviation δ obeys U (1,1.2). The vibration signal s_3 satisfies the following expression:

$$s_3 = A_1\sin(30\pi t) + A_2\cos(40\pi t) + A_3\sin(50\pi t + \pi/4). \tag{30}$$

where A_1 obeys N (0.7,0.7^2), A_2 obeys N (0.4,0.4^2) and A_3 obeys N (0.3,0.3^2).

The signal s satisfies the following expression:

$$s = s_1 + s_2 + s_3. \tag{31}$$

The sampling frequency fs_1 = 1024 Hz simulates the higher measurement rate of the accelerometer. The sampling frequency fs_2= 256 Hz simulates the attitude sensor with low measurement rate. Take the b = 0.99 in equation (26).

To verify the effectiveness of vibration analysis method, the results of FLAKF method and the proposed estimation method are compared. The simulation results are shown in Figure 9.

According to Figure 9, the estimation error based on direct FLAKF is larger. The estimation method based on SDFT and FLAKF in this paper can effectively improve the estimation precision.

To quantify the estimation accuracy, the root mean square error (RMSE) is used to evaluate the estimated results. The

Figure 9 The simulation results of direct FLAKF and the proposed estimation method

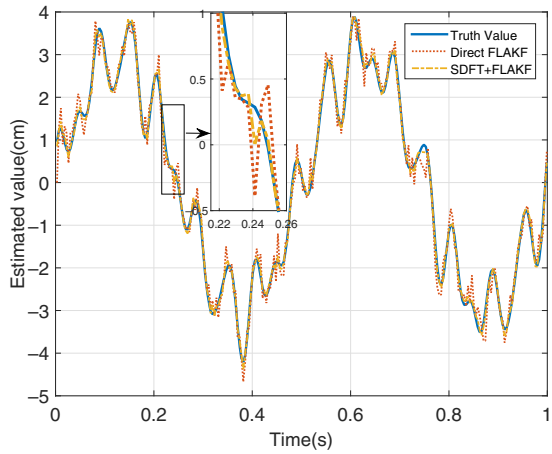

results of the RMSE are shown in Table II. It can be seen that the error of the proposed method in this paper is obviously reduced from Table II.

To verify the effectiveness of the FLAKF algorithm, the traditional EKF algorithm and the proposed FLAKF in this paper are used to estimate the data after filtering in frequency domain respectively. The simulation results are shown in Figure 10.

Because of the random noise in the amplitude, the noise still exists after filtering in the frequency domain. The simulation results show that the estimation error of using EKF is obviously greater than the FLAKF. The RMSE is shown in Table III, and it verifies the effectiveness of the proposed FLAKF in this paper directly.

4.2 Experimental setup

In this paper, a HSFM experimental setup with a telescopic joint and a rotating joint is designed, and the corresponding data are obtained by the sensors. The design drawings and the actual setup are as shown in Figure 11.

The experimental system consists of two parts: the flexible manipulator system and the sensor system. The flexible manipulator system includes steel base platform, motor holder, 200/100 W Panasonic servo motor, motor driver, coupling, first flexible link, second flexible link, screw, linear bearing, Trio motion controller and so on. The sensor system includes accelerometer, attitude sensor and data acquisition card. The flexible link adopts a nested structure. The length of first flexible link is 1000 mm, and the length of second flexible link is 1200 mm, all of which are made of aluminum alloy. The tip of the first flexible link is equipped with a straight line bearing for fixing the second flexible link. The second flexible link is connected to the servo motor by a guide screw and a slider. The output shaft of the 200 W Panasonic servo motor connects the

Table II Root mean square error of direct FLAKF and SDFT + FLAKF

Method	RMSE
Driect FLAKF	0.2724
SDFT + FLAKF	0.0979

Figure 10 The simulation results of EKF and FLAKF after filtering in frequency domain

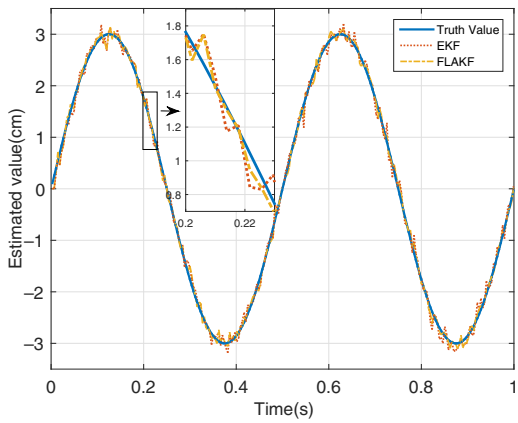

Table III Root mean square error of EKF and FLAKF

Method	RMSE
EKF	0.1269
FLAKF	0.0946

harmonic reducer with a reduction ratio of 80. The output of the harmonic reducer is used to drive the HSFM to rotate in the vertical plane. The 100 W Panasonic servo motor is used to drive second flexible link for telescopic motion. The servo motor has 22 bits encoder, which record the angular position of the motor rotation accurately. Accelerometer and the attitude sensor are installed at the tip of the flexible link. The output signal of the accelerometer is converted to digital signal through the data acquisition card. The attitude sensor uses bluetooth communication mode to transfer the tip state back to the PC.

4.3 Experimental results of open loop control

The experiment is carried out on the experimental platform described in the previous section. The five-order polynomial functions are used as the joint reference trajectories. The open loop control method is used to rotate the tip of HSFM from the horizontal position to the vertical position, and the telescopic joint moves 150 mm from the minimum position. The tip state signals are collected by sensors and analyzed. The spectrum diagram of the tip acceleration signal is obtained and shown in Figure 12. The tip vibration frequency of is mainly concentrated near 3 Hz according to Figure 12.

The estimate results of the FLAKF and the proposed estimator are shown in Figures 13-15. These results show that the tip state curve obtained by the proposed state estimator is smoother, and the random disturbance is smaller. The SDFT is more accurately to get the main vibration components of the tip and filter the high frequency vibration noise. The vibration of the telescopic joint is obviously less than the vibration of the rotating joint, which is consistent with the assumption that the vibration in the model is mainly in the direction of rotation.

The tip angular velocity is selected to verify the effectiveness of the proposed FLAKF algorithm. The original measurement signal is filtered in the frequency domain, and the tip angular velocity is estimated. The estimated results obtained by using EKF and the proposed FLAKF in this paper are shown in Figure 16.

The main vibration components of the angular velocity are shown in Figure 17. In the process of motion, the vibration is superimposed by multiple frequencies, and the amplitude and frequency vary with time.

4.4 Experimental results of closed loop control

The proposed estimator and the EKF estimator are used in the control system introduced in the Section 3.4. The estimate value and the reference value are compared to verify the effectiveness of the estimator. According to the results of the open loop control experiment, the tip vibration is mainly in the direction of rotation, so the tip state in the rotation direction is only compared in this section. The results of the experiment are shown in Figure 18.

According to the experimental results, the tracking effect of the EKF estimator is always inferior to the proposed estimator in different trajectories. To quantify the tracking error, the RMSE is used to analyze and compare these experimental results, which are shown in Table IV. According to RMSE data, the proposed estimator has a better tracking effect, which illustrates the effectiveness of the proposed estimator indirectly. On the other hand, comparing the trajectory tracking curves of the two groups, we can see that the longer movement time of the unit angle, the smaller amplitude of vibration and the better tracking performance.

5. Conclusion

To solve the problem that the tip state of the HSFM in the vertical plane is difficult to be measured, a tip state estimator

Figure 11 Experimental setup

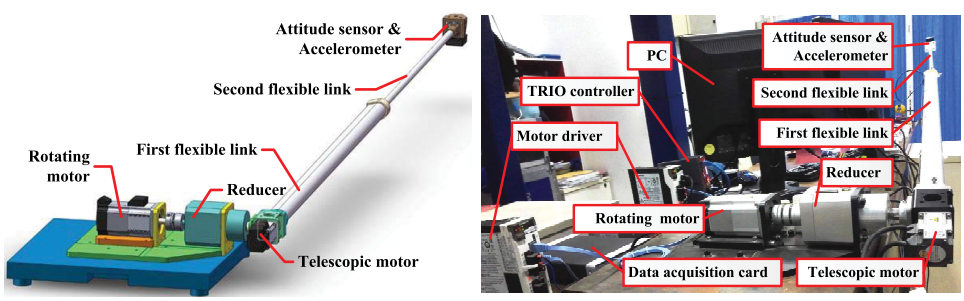

Figure 12 Spectrum diagram of tip acceleration signal

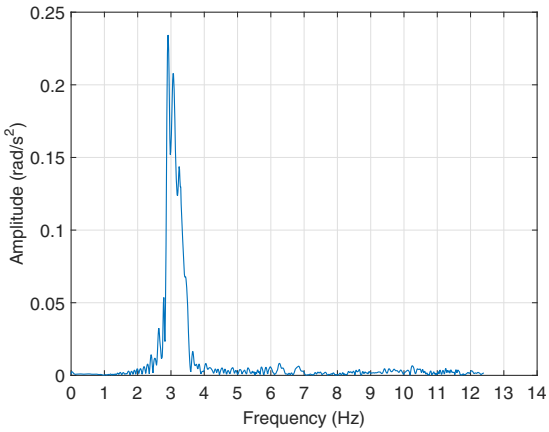

Figure 13 The angular position and the telescopic position of the tip in open control experiment

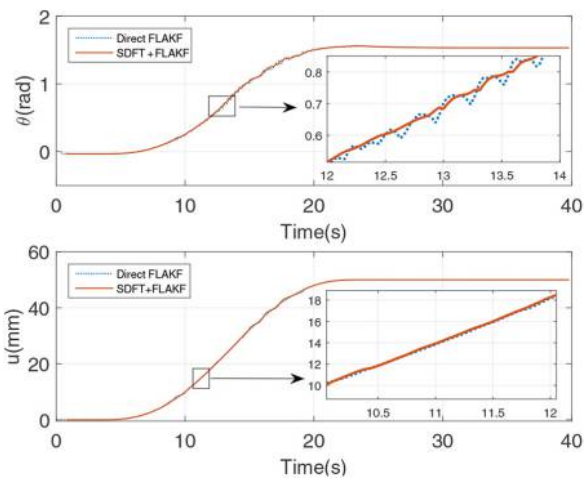

Figure 14 The angular velocity and the telescopic speed of the tip in open control experiment

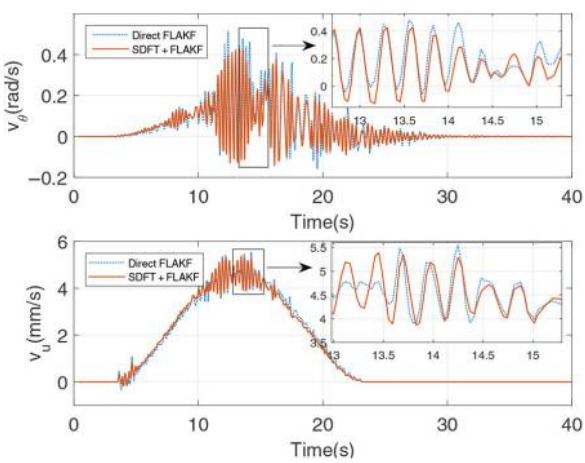

Figure 15 The angular acceleration and the telescopic acceleration of the tip in open control experiment

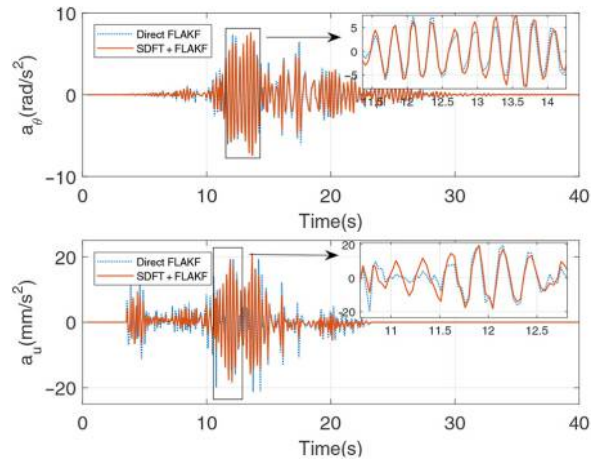

Figure 16 The angular velocity after filtering in frequency domain in open loop control experiment

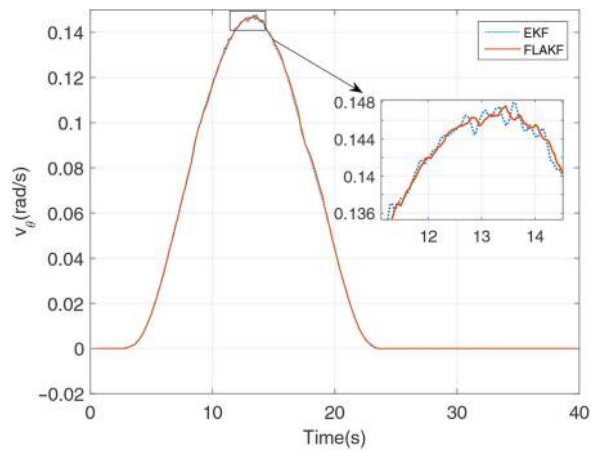

Figure 17 The main vibration component of the angular velocity

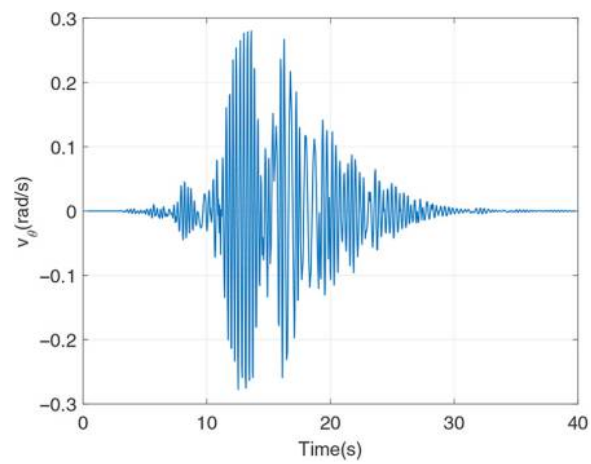

Figure 18 Tip tracking effect of different trajectories in closed loop control experiments

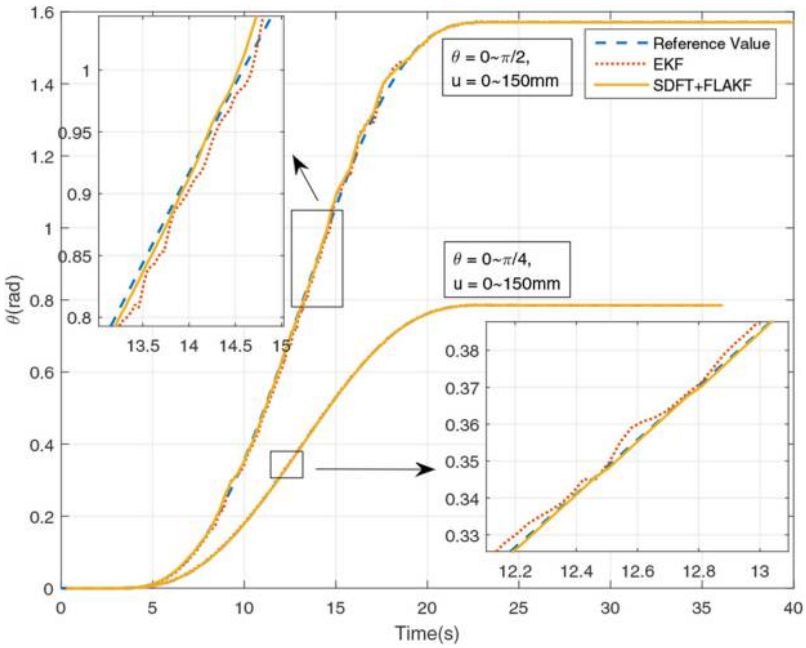

Table IV Root mean square error of trajectory tracking

Method	RMSE($\pi/2$)	RMSE($\pi/4$)
EKF	0.0087	0.0018
SDFT + FLAKF	0.0071	0.00052

based on SDFT and FLAKF is designed in this paper. The main work is generalized as follows:

- The static deflection model of the HSFM is established to calculate the tip elastic deformation, which can effectively improve the estimation accuracy and reduce the computational complexity in the estimation process.
- The vibration analysis based on SDFT is used to represent the vibration model and avoid the complicated computational process of differential equation. The proposed SDFT algorithm can accurately estimate the amplitude and frequency of the signal and has strong robustness.
- Based on the Sage–Husa adaptive Kalman filter algorithm, a FLAKF algorithm is designed to increase the stability and robustness of the estimator.
- The experiment is designed to verify the effectiveness of the proposed estimator and the FLAKF algorithm.

The estimator designed in this paper is an important part of the research process of the vibration suppression control of the HSFM in the vertical plane. It is used to get the precise tip state of the HSFM and evaluate the performance of the control system.

In future research, different load conditions will be taken into consideration to further improve the robustness of the state estimator, and the estimator will verify its effectiveness on the actual flexible manipulator system.

References

Abe, A. (2010), "Trajectory planning for flexible cartesian robot manipulator by using artificial neural network: numerical simulation and experimental verification", *Robotica*, Vol. 29 No. 5, pp. 797-804.

Benosman, M. and Le Vey, G. (2004), "Control of flexible manipulators: a survey", *Robotica*, Vol. 22 No. 5, pp. 533-545.

Benosman, M., Le Vey, G., Lanari, L., *et al.* (2003), "Rest-to-rest motion for planar multi-link flexible manipulator", *IFAC Proceedings Volumes*, Vol. 36 No. 17, pp. 289-294.

Bian, H., Jin, Z., Wang, J., et al. (2006), "The innovation-based estimation adaptive kalman filter algorithm for ins/gps integrated navigation system", *Journal of Shanghai Jiaotong University*, Vol. 40 No. 6, pp. 1000-1003, 1009.

Bosman, J., Bieze, T., Lakhal, O., *et al.* (2015), "Domain decomposition approach for FEM quasistatic modeling and control of continuum robots with rigid vertebras", in 2015 IEEE International Conference on Robotics and Automation (ICRA) in Seattle, Washington, DC, 26-30 May, pp. 4373-4378.

Carlos, J. and Feliu, V. (2017), "Input-state feedback linearization control of a single-link flexible robot arm moving under gravity and joint friction", *Robotics and Autonomous Systems*, Vol. 88, pp. 24-36.

Chen, W. (2001), "Dynamic modeling of multi-link flexible robotic manipulators", *Computers & Structures*, Vol. 79 No. 2, pp. 183-195.

Chen, Z., Yang, C., Liu, X., *et al.* (2017), "Learning control of flexible manipulator with unknown dynamics", *Assembly Automation*, Vol. 37 No. 3, pp. 304-313.

Coelho, B., Holscher, P. and Barends, F. (2011), "Enhancement of double integration procedure through

spectral subtraction", *Soil Dynamics and Earthquake Engineering*, Vol. 31 No. 4, pp. 716-722.

Dwivedy, S.K. and Eberhard, P. (2006), "Dynamic analysis of flexible manipulators, a literature review", *Mechanism and Machine Theory*, Vol. 41 No. 7, pp. 749-777.

Feliu, V., Castillo, F.J., Ramos, F., *et al.* (2012), "Robust tip trajectory tracking of a very lightweight single-link flexible arm in presence of large payload changes", *Mechatronics*, Vol. 22 No. 5, pp. 594-613.

Hou, M. (2005), "Amplitude and frequency estimator of a sinusoid", *IEEE Transactions on Automatic Control*, Vol. 50 No. 6, pp. 855-858.

Hsu, L., Ortega, R. and Damm, G. (1999), "A globally convergent frequency estimator", *IEEE Transactions on Automatic Control*, Vol. 44 No. 4, pp. 698-713.

Jacobsen, E. and Lyons, R. (2003), "The sliding DFT", *IEEE Signal Processing Magazine*, Vol. 20 No. 2, pp. 74-80.

Jacobsen, E. and Lyons, R. (2004), "An update to the sliding DFT", *IEEE Signal Processing Magazine*, Vol. 21 No. 1, pp. 110-111.

Kiang, C.T., Spowage, A. and Yoong, C.K. (2015), "Review of control and sensor system of flexible manipulator", *Journal of Intelligent & Robotic Systems*, Vol. 77 No. 1, pp. 187-213.

Liu, C., Xiang, X. and Poignet, P. (2011), "Adaptive tracking control of rigid-link flexible-joint robot manipulator with uncertainties", *IFAC Proceedings Volumes*, Vol. 44 No. 1, pp. 10300-10306.

Long, T., Li, E., Yang, G., et al. (2016), "A novel model analysis method and dynamic modelling for hybrid structure flexible manipulator", in 2016 IEEE International Conference on Mechatronics and Automation (ICMA) in Haerbin, China, 7-10 August, pp. 2290-2295.

Lou, J., Wei, Y., Li, G., *et al.* (2015), "Optimal trajectory planning and linear velocity feedback control of a flexible piezoelectric manipulator for vibration suppression", *Shock and Vibration*, Vol. 2015, pp. 1-11.

Lu, P., Zhao, L. and Chen, Z. (2007), "Improved Sage-Husa adaptive filtering and its application", *Journal of System Simulation*, Vol. 15, pp. 3503-3505.

Makarov, M., Grossard, M., Rodriguez-Ayerbe, P., *et al.* (2012), "Active damping strategy for robust control of a flexible-joint lightweight robot", in 2012 IEEE International Conference on Control Applications (CCA) in Dubrovnik, Croatia, 3-5 October, pp. 1020-1025.

Malgaca, L., Yavuz, A., Akdag, M., *et al* (2016), "Residual vibration control of a single-link flexible curved manipulator", *Simulation Modelling Practice and Theory*, Vol. 67, pp. 155-170.

Mirzaee, E., Eghtesad, M. and Fazelzadeh, S.A. (2010), "Maneuver control and active vibration suppression of a two-link flexible arm using a hybrid variable structure lyapunov control design", *Acta Astronautica*, Vol. 67 Nos 9/10, pp. 1218-1232.

Sayahkarajy, M., Mohamed, Z. and Faudzi, A.A.M. (2016), "Review of modelling and control of flexible-link manipulators", *Proceedings of the Institution of Mechanical Engineers Part I-Journal of Systems and Control Engineering*, Vol. 230 No. 8, pp. 861-873.

Shitole, C. and Sumathi, P. (2015), "Sliding DFT-based vibration mode estimator for single-link flexible manipulator", *IEEE/ASME Transactions on Mechatronics*, Vol. 20 No. 6, pp. 3249-3256.

Sooraksa, P. and Chen, G. (1998), "Mathematical modeling and fuzzy control of a flexible-link robot arm", *Mathematical and Computer Modelling*, Vol. 27 No. 6, pp. 73-93.

Sumathi, R. and Janakiraman, P.A. (2008), "Integrated phase-locking scheme for sdft-based harmonic analysis of periodic signals", *IEEE Transactions on Circuits and Systems II: Express Briefs*, Vol. 55 No. 1, pp. 51-55.

Trapero, J.R., Sira, H. and Feliu, V. (2007), "An algebraic frequency estimator for a biased and noisy sinusoidal signal", *Signal Processing*, Vol. 87 No. 6, pp. 1188-1201.

Turner, C.S. (2003), "Recursive discrete-time sinusoidal oscillators", *IEEE Signal Processing Magazine*, Vol. 20 No. 3, pp. 103-111.

Vartanov, M.V., Bojkova, L.V. and Zinina, I.N. (2017), "Mathematical model of robotic assembly by means of adaptation and low-frequency vibration", *Assembly Automation*, Vol. 37 No. 1, pp. 130-134.

Yang, Y. and Gao, W. (2006), "An optimal adaptive kalman filter", *Journal of Geodesy*, Vol. 80 No. 4, pp. 177-183.

Yang, B., Liu, C., Zheng, W., *et al* (2017), "Motion prediction via online instantaneous frequency estimation for vision-based beating heart tracking", *Information Fusion*, Vol. 35, pp. 58-67.

Yang, H.J. and Tan, M. (2018), "Sliding mode control for flexible-link manipulators based on adaptive neural networks", *International Journal of Automation and Computing*, Vol. 2018, pp. 1-10.

Yavuz, S., Malgaca, L. and Karagulle, H. (2016), "Vibration control of a single-link flexible composite manipulator", *Composite Structures*, Vol. 140, pp. 684-691.

Yi, T., Li, H. and Gu, M. (2010), "Recent research and applications of gps based technology for bridge health monitoring", *Science China Technological Sciences*, Vol. 53 No. 10, pp. 2597-2610.

Zhu, G., Ge, S.S. and Lee, T.H. (1999), "Simulation studies of tip tracking control of a single-link flexible robot based on a lumped model", *Robotica*, Vol. 17 No. 1, pp. 71-78.

Ziarani, A.K. and Konrad, A. (2004), "A method of extraction of nonstationary sinusoids", *Signal Processing*, Vol. 84 No. 8, pp. 1323-1346.

Corresponding author

En Li can be contacted at: en.li@ia.ac.cn